Fast Ca^{2+} responses in astrocyte end-feet and neurovascular coupling in mice

Barbara Lykke Lind, Sanne Barsballe Jessen, Micael Lønstrup, Charlène Joséphine, Gilles Bonvento, Martin Lauritzen

Received: 27 April 2017 | Revised: 28 September 2017 | Accepted: 29 September 2017

DOI: 10.1002/glia.23246

GLIA
WILEY

RESEARCH ARTICLE

Fast Ca^{2+} responses in astrocyte end-feet and neurovascular coupling in mice

Barbara Lykke Lind[1] | Sanne Barsballe Jessen[1] | Micael Lønstrup[1] | Charlène Joséphine[2] | Gilles Bonvento[2] | Martin Lauritzen[1,3]

[1]Department of Neuroscience and Center for Healthy Aging, University of Copenhagen, Denmark

[2]Commissariat à l'Energie Atomique et aux Energies Alternatives (CEA), Département de la Recherche Fondamentale (DRF), Institut de Biologie François-Jacob, Molecular Imaging Research Center (MIRCen), CNRS UMR 9199, Université Paris-Sud, Université Paris-Saclay, Fontenay-aux-Roses, France

[3]Department of Clinical Neurophysiology, Glostrup Hospital, Denmark

Correspondence
Barbara Lykke Lind, Center for Neuroscience, Mærsk Tower niveau 4, Blegdamsvej 3, DK-2200 Copenhagen N, Denmark (or) DNF, University of Lausanne, Rue du Bugnon 9, 1005 Lausanne, Suisse.
Email: barbaral@sund.ku.dk (or) BarbaraLykke.Lind@unil.ch

Funding information
The Lundbeck Foundation; The NOVO-Nordisk Foundation; The Danish Medical Research Council; The NORDEA Foundation for the Center for Healthy Aging; Fondation Leducq

Abstract

Cerebral blood flow (CBF) is regulated by the activity of neurons and astrocytes. Understanding how these cells control activity-dependent increases in CBF is crucial to interpreting functional neuroimaging signals. The relative importance of neurons and astrocytes is debated, as are the functional implications of fast Ca^{2+} changes in astrocytes versus neurons. Here, we used two-photon microscopy to assess Ca^{2+} changes in neuropil, astrocyte processes, and astrocyte end-feet in response to whisker pad stimulation in mice. We also developed a pixel-based analysis to improve the detection of rapid Ca^{2+} signals in the subcellular compartments of astrocytes. Fast Ca^{2+} responses were observed using both chemical and genetically encoded Ca^{2+} indicators in astrocyte end-feet prior to dilation of arterioles and capillaries. A low dose of the NMDA receptor antagonist (5R,10s)-(+)-5-methyl-10,11-dihydro-5H-dibenzo[a,d]cyclohepten-5,10-imine-hydrogen-maleate (MK801) attenuated fast Ca^{2+} responses in the neuropil and astrocyte processes, but not in astrocyte end-feet, and the evoked CBF response was preserved. In addition, a low dose of 4,5,6,7-tetrahydroisoxazolo[5,4-c]pyridin-3-ol (THIP), an agonist for the extrasynaptic $GABA_A$ receptor ($GABA_AR$), increased CBF responses and the fast Ca^{2+} response in astrocyte end-feet but did not affect Ca^{2+} responses in astrocyte processes and neuropil. These results suggest that fast Ca^{2+} increases in the neuropil and astrocyte processes are not necessary for an evoked CBF response. In contrast, as local fast Ca^{2+} responses in astrocyte end-feet are unaffected by MK801 but increase via $GABA_AR$-dependent mechanisms that also increased CBF responses, we hypothesize that the fast Ca^{2+} increases in end-feet adjust CBF during synaptic activity.

KEYWORDS
astrocyte end-feet, calcium imaging, blood flow regulation, in vivo, pixel detection

1 | INTRODUCTION

Changes in brain activity are accompanied by changes in brain metabolism and perfusion. This relationship is the basis of functional neuroimaging techniques that use deviations in cerebral blood flow (CBF) or blood oxygenation level–dependent signals to track brain activity (Lauritzen, Mathiesen, Schaefer, & Thomsen, 2012; Logothetis, Pauls, Augath, Trinath, & Oeltermann, 2001; Raichle & Mintun, 2006). Activity-dependent increases in CBF are thought to be regulated by Ca^{2+} increases in neurons and astrocytes (Attwell et al., 2010; Devor et al., 2003; Gordon, Choi, Rungta, Ellis-Davies, & MacVicar, 2008; Howarth, 2014; Iadecola & Nedergaard, 2007; McCaslin, Chen, Radosevich, Cauli, & Hillman, 2011; Petzold, Albeanu, Sato, & Murthy, 2008). Astrocyte processes are in close contact with synapses (Nimmerjahn, 2009), and astrocyte end-feet cover neighboring vessels (Kacem, Lacombe, Seylaz, & Bonvento, 1998; McCaslin et al., 2011). Thus, astrocytes are optimally placed to link increases in synaptic activity to increases in CBF. The timing and reliability of astrocyte Ca^{2+} responses are controversial (Nizar et al., 2013; Winship, Plaa, & Murphy, 2007), but we have reported that the majority of astrocytes have fast Ca^{2+} responses prior to hemodynamic responses within 300 ms of synaptic activation (Lind, Brazhe, Jessen, Tan, & Lauritzen, 2013). The mechanisms underlying the fast change in Ca^{2+} in astrocytes have not been clarified, though several have been proposed (Verkhratsky,

Rodriguez, & Parpura, 2012; Volterra, Liaudet, & Savtchouk, 2014). *In vivo* astrocytic Ca^{2+} responses have been studied primarily in the astrocyte soma, though the dynamics of Ca^{2+} responses in the astrocyte processes and end-feet differ from somatic responses (Bindocci et al., 2017; Kanemaru et al., 2014; Reeves, Shigetomi, & Khakh, 2011; Srinivasan et al., 2015; Stobart et al., 2016). In addition, astrocytes can be compartmentalized, with one part of a cell responding independently from its other parts (Bindocci et al., 2017; Shigetomi et al., 2013). Fast Ca^{2+} responses in astrocyte processes may influence synaptic transmission, affecting the activity in nerve networks (Di Castro et al., 2011; Panatier et al., 2011). Stimulation-induced Ca^{2+} responses in astrocyte end-feet are of great interest for neurovascular coupling because they have been found to influence vascular diameter in slices (Dunn, Hill-Eubanks, Liedtke, & Nelson, 2013; Gordon et al., 2008) and to occur prior to vasodilatation *in vivo* (Lind et al., 2013; Otsu et al., 2015; Petzold et al., 2008).

Here, we compare the fast Ca^{2+} responses in neuropil and astrocyte processes to those in astrocyte end-feet during whisker pad stimulation of the mouse barrel cortex. Importantly, the astrocytic source of the fast Ca^{2+} changes was verified using a genetically encoded, astrocyte-specific Ca^{2+} indicator. Fast Ca^{2+} increases in neuropil and astrocyte processes depended on preserved NMDA receptor (NMDAR) activity but were unnecessary for the development of a CBF response. In contrast, local Ca^{2+} increases in astrocyte end-feet were unaffected by the NMDAR antagonist (5R,10s)-(+)-5-methyl-10,11-dihydro-5H-dibenzo[a,d]cyclohepten-5,10-imine-hydrogen-maleate (MK801) but increased with exposure to a low dose of 4,5,6,7-tetrahydroisoxazolo [5,4-c]pyridin-3-ol (THIP), which tonically activates extrasynaptic $GABA_A$ receptors ($GABA_A$Rs). The same dose of THIP also enhanced the CBF response. These *in vivo* data support the participation of fast Ca^{2+} responses in astrocyte end-feet in the translation of synaptic input into a vascular signal.

2 | MATERIALS AND METHODS

2.1 | Experimental setup

All procedures involving animals were approved by the Danish National Ethics Committee according to the guidelines set forth in the European Council's Convention for the Protection of Vertebrate Animals Used for Experimental and Other Scientific Purposes and to the ARRIVE guidelines. Forty-seven male white Naval Medical Research Institute mice [8 weeks old, Crl:NMRI (male)] were surgically prepared for experiments, and a craniotomy was performed. A total of 37 of these animals were used for the two-photon microscopy experiments. An additional 10 animals were used to study blood flow in a separate experimental setup.

The mouse sensory barrel cortex was activated by electrical stimulation of the contralateral ramus infraorbitalis of the trigeminal nerve in trains of 15 s at 0.5–5 Hz. The trains of stimulations were repeated three times for each frequency in each animal. In three mice, air puffs lasting 0.2 ms were applied to the whiskers at similar stimulation frequencies. In the whisker cortex layer II/III, the extracellular local field potentials (LFPs) were recorded to measure field excitatory postsynaptic potential (fEPSP). The hemodynamic responses were measured by intrinsic optical signals or monitored using laser Doppler flowmetry. Ca^{2+} imaging was performed using two-photon microscopy. In 27 mice, the tissue was loaded with the red astrocyte-specific dye sulforhodamine 101 (SR101) in combination with the green fluorescent Ca^{2+} indicator Oregon Green Bapta (OGB)-1/AM (OGB-1/AM), while in 10 mice, a genetically encoded green fluorescent GCaMP6f Ca^{2+} indicator under the astrocyte-specific glial fibrillary acidic protein promoter was virally introduced 2–4 weeks prior to the imaging. For further information on the animal handling, viral injections, immunohistochemistry, stimulation, electrophysiology, cortical blood flow, two-photon imaging, post-sampling analysis of vessel diameter, and details on image analysis, refer to the Supporting Information.

2.2 | Image analysis

A series of OGB/SR101 images were taken before and during whisker pad stimulation. Several square sections were cropped from each image, each containing either an astrocyte process or astrocyte end-feet (Figure 1a and Supporting Information Fig. S1a). The series of cropped images was rearranged as previously described (Lind et al., 2013) using the stimulation time as a time lock; data points were superimposed to form a cloud of data points as though they were obtained after a single stimulation (Supporting Information Fig. S1b). An average series of images was interpolated from the green Ca^{2+} indicator channel and red SR101 channel of the original image sections (Supporting Information Fig. S1c). Areas were identified as astrocytic or nonastrocytic based on the level of SR101 staining in the interpolated image (Supporting Information Fig. S1d). We used a threshold of 1 standard deviation (s.d.) to separate astrocytic from nonastrocytic pixels because interpolation of the signal reduces variation. The precision of this threshold was confirmed by evaluating the spread of SR101 loading in astrocytic versus nonastrocytic pixels (Figure 1b) in 23 series of image frames from six animals.

The SR101-based selection of pixels of interest (POIs) was repeated in each image in the interpolated time series. Thus, all pixels within each frame were reevaluated as part of either the astrocytic or nonastrocytic POIs. The fluorescence activity in the green channel reflected Ca^{2+} levels and the mean value was calculated for each class of pixels and taken to represent the level of Ca^{2+} inside or outside the entire astrocyte structure at a given time point (Supporting Information Fig. S1e). The average fast Ca^{2+} responses to whisker pad stimulation could be evaluated because the Ca^{2+} responses were visualized by linear interpolation over data points from the same POI, image to image (Supporting Information Fig. S1f). The mean fluorescence and s.d. during the baseline period was used to normalize the values in the entire time series. The normalization was calculated as the percentage of the baseline level ($\Delta F/F_0$) and the s.d. of baseline activity ($\Delta F_{s.d.} = \Delta F - F_0/s.d._0$).

Next, the fast Ca^{2+} response was analyzed with regard to timing, maximum peak amplitude, and whether the response was significantly larger than baseline, defined as at least four data points above 2 s.d. of

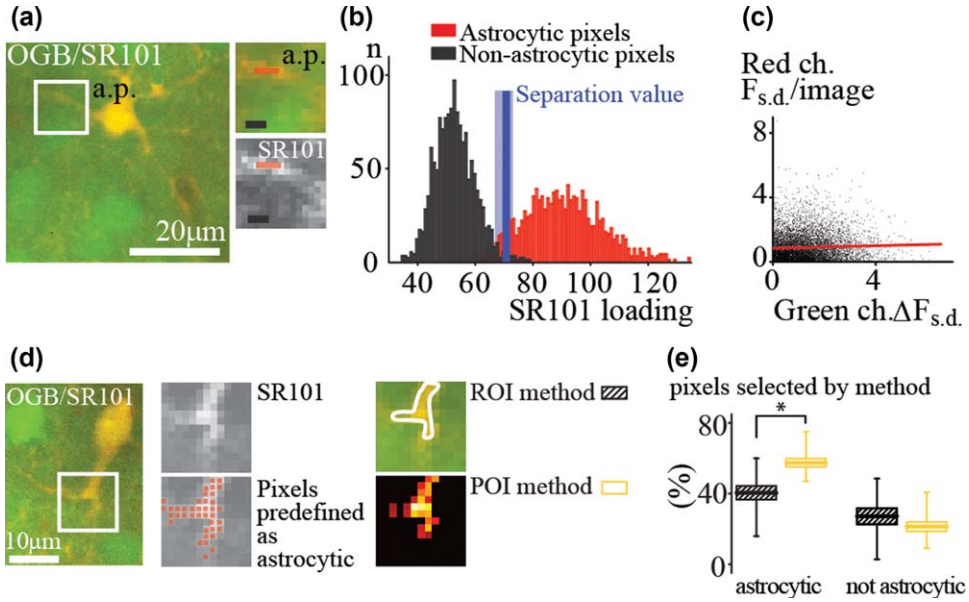

FIGURE 1 Unbiased pixel-based selection of astrocyte-specific fluorescence shows high sensitivity. Categorization of pixels as astrocytic versus non-astrocytic was based on SR101 levels from image to image. (**a**) Astrocyte process isolated in a rectangular section (white square). The excerpt shows the OGB/SR101 image (top) and SR101 channel (bottom). (**b**) Distribution of SR101 expression in the pixels specified by the red and dark gray lines (a). The distributions are shown for a series of scans. The cross point of overlap between the two distributions matched the separation value (dark blue line). The light blue section indicates the range of separation values observed in 23 other experiments. (**c**) The size of the stimulation-induced Ca^{2+} changes measured in the green channel did not correlate with the level of SR101 detection in the red channel. Thus, the fluorescence increase from OGB did not influence the classification of astrocytic POIs. (**d**) ROI and POI methods were applied to the same dataset. First, astrocytic pixels were selected manually (red dots). Second, we applied the POI method to the same image in a blinded fashion. (**e**) The POI method was more sensitive than the ROI method in detecting astrocytic pixels ($n = 12$, $p < 0.001$, t-test)

baseline activity. The response was smoothed to enable the estimation of onset time by calculating the maximum value in the second derivative, and of decay time by determining when the signal dropped below baseline levels. Analytical software was developed using Matlab™.

2.3 | Drug application

CNQX, MK801, and THIP were dissolved in artificial cerebrospinal fluid and applied by placing drops of the dissolved compound on the agarose covering the cortex. Further information about these drugs is given in the Supporting Information.

2.4 | Statistical analysis

The drug effects on fEPSP and CBF responses, as well as the size and timing of fast Ca^{2+} signals, were analyzed using three-way analysis of variance (ANOVA; R, R Development Core Team 2010; R Foundation for Statistical Computing, Vienna, Austria) on the range of stimulation frequencies applied (0.5–5 Hz), followed by a paired t-test for significance at a specific stimulation frequency. The significance level was set at a two-tailed α of 0.05. In some cases, data were log-transformed before analysis to obtain a normal distribution. All studies were paired to ensure that the control measurements were carried out in the same animals that would later be exposed to a drug.

Part of the dataset for 24 of the 37 mice examined by two-photon microscopy imaging was published in two previous papers (Jessen et al., 2014; Lind et al., 2013). Those studies involved another analytical method for evaluating Ca^{2+} changes, and neither reported the drug effects on fast Ca^{2+} responses in astrocyte processes or end-feet.

2.5 | Comparison of the ROI and POI methods

To compare the sensitivity of the POI and region of interest (ROI) methods to correctly select astrocytic pixels, the two approaches were applied to a dataset in which the ideal classification of pixels was known. This dataset was developed through manual evaluation of 12 different series of frames in four animals, and each astrocytic pixel was designated based on a combination of visually selecting adjacent pixels and the intensity of SR101 loading. A total of 732 frames were reviewed and then submitted to automatic pixel selection by the ROI and POI methods. The percent of astrocytic pixels correctly identified by each method was calculated, as well as the percent of pixels selected by either method that were not astrocytic (Figure 1d).

3 | RESULTS

We previously provided evidence for fast stimulation-induced Ca^{2+} responses in astrocyte structures in layer II/III of the whisker barrel cortex using the Ca^{2+} indicator OGB (Lind et al., 2013). In that study, our analysis was based on the mean fluorescence activity within ROIs selected based on staining with the astrocyte-specific marker SR101,

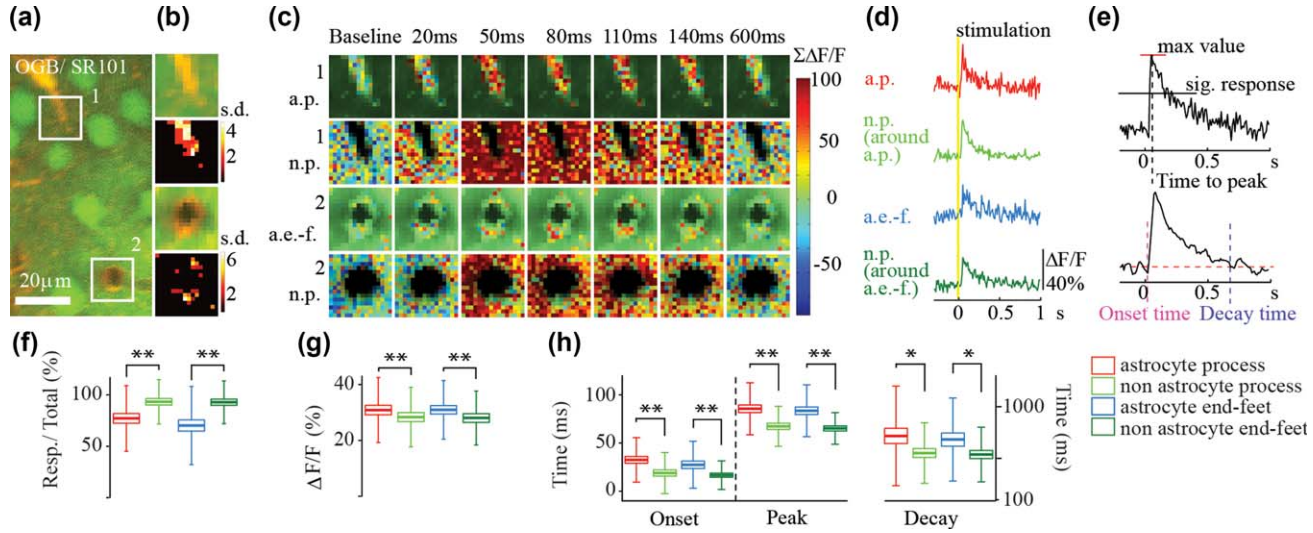

FIGURE 2 Pixel-based analysis of the whisker pad stimulation induced fast Ca^{2+} responses in astrocyte processes and end-feet. (**a**) Layer II/III of whisker barrel cortex, SR101: astrocyte-specific (red), OGB: Ca^{2+} fluorophore (green). (**b**) Small astrocyte structures were separated from the surrounding neuropil as POIs. The excerpts from the two white squares (a) are shown above the images of the selected POIs. (**c**) Ca^{2+}-dependent fluorescence changes in astrocytic and non-astrocytic structures. A time series of stimulation-evoked Ca^{2+} increases in an astrocyte process (a.p.), astrocyte end-foot (a.e.-f.), the neuropil around the astrocyte processes (n.p. around a.p.), and the neuropil around the end-foot (n.p. around a.e.-f.). The color scale show the size of the Ca^{2+} responses in % of baseline Ca^{2+} activity ($\Delta F/F_0$) summed over 30 ms intervals. (**d**) The fast Ca^{2+} response from each of the four areas in (c). Zero indicates the onset of stimulation. (**e**) The fast Ca^{2+} signal fitted to calculate onset and decay time. (**f**) The percentage of ROIs responding with a fast Ca^{2+} signal (>2 $F_{s.d.}$ of baseline activity) was significantly higher in neuropil than in astrocyte structures. (**g**) Fast Ca^{2+} responses were significantly larger in astrocyte structures than in the associated neuropil. (**h**) The timing of the fast Ca^{2+} signal was significantly faster in the neuropil than in astrocyte structures in terms of onset time, peak time, and decay time. Data from 15 s, 0.5 Hz stimulations ($n = 48$ structures, 24 animals). Boxplots show mean (line), s.d. (box), and s.e.m. (whiskers). * $p < 0.05$, ** $p < 0.01$, *t*-test

cell morphology, and connection to blood vessels. With regard to smaller structures, such as astrocyte processes and end-feet, this procedure may be less satisfactory because of the imperfect fit of a ROI and the low number of pixels measured in the structure. To address this issue, we developed an analytical method by which POIs are defined based on the intensity of SR101 detected in individual pixels (Supporting Information Fig. S1). This approach increased the sensitivity, as more pixels in a small structure could be included in the study.

The first step was to isolate a rectangular section of image that contained only the astrocyte structure to be evaluated (Figure 1a). This step was necessary because the uptake of dye is sometimes dissimilar over a field of view and between astrocyte somas and processes. Thus, with the inclusion of only a single astrocyte structure within the section, the algorithm that defined the pixels with significant SR101 levels was applied to more homogeneous SR101 staining and achieved greater accuracy. All pixels with significant SR101 levels were classified as astrocytic, whereas the rest were considered to be nonastrocytic. For each section of an image, a separation value was determined for significant SR101 staining. The accuracy of this value was verified by comparing the distribution of SR101 levels in two clusters of pixels within the same image section containing either only astrocytic or nonastrocytic pixels (Figure 1b).

In the investigated series of image sections, we found that the separation value matched the cross point between the two distributions or had a tendency toward the SR101 mean; this outcome was what we had aimed for to minimize the number of nonastrocytic pixels among astrocytic pixels. Next, for each pixel, we compared the size of the Ca^{2+} responses during whisker pad stimulation and the level of SR101 detected during that response (Figure 1c). We included this comparison because of the unavoidable contribution of OGB emission to the SR101 signal; OGB emits light in the red spectrum even though its primary emission is in the green spectrum. No relationship was found between detected SR101 levels and the size of the shift in OGB emission, indicating that no pixels changed status from nonastrocytic to astrocytic as a result of enhanced Ca^{2+} levels during stimulation.

For a direct comparison of the accuracy of the POI and ROI methods, we applied both to a set of data in which the precise numbers and positions of astrocytic pixels were predefined by manual/visual scoring (Figure 1d). The POI method had significantly higher sensitivity ($n = 12$, $p < 1 \times 10^{-3}$, *t*-test) by selecting 57.4 ± 4.5% of the pixels pre-defined as astrocytic; the ROI method selected only 40.4 ± 7.4%. However, the specificities of the two methods were comparable. Of the pixels selected by the POI method, 21.3 ± 4.9% were not predefined as astrocytic; this was true for 27.2 ± 8.5% of the selected pixels with the ROI methods (Figure 1e).

Next, we evaluated the fast Ca^{2+} responses within astrocyte processes and end-feet calculated from the activity during a train of whisker pad stimulations (Figure 2a). The type of astrocyte structure was already defined in the section selection process based on morphology (Figure 2b). The separation of pixels by the POI method created two

TABLE 1 Mean values for 0.5 Hz stimulations and 95% confidence limits

	Ca^{2+} indicator	Maximum amplitude (%)	Responsivity (%)	Onset time (ms)	Peak time (ms)	Decay time (ms)
Astrocyte processes	OGB	30.9 ± 3.3	77.1 ± 8.9	33 ± 7	86 ± 8	717 ± 136
Neuropil	OGB	28.3 ± 2.9	93.3 ± 6.0	19 ± 6	67 ± 6	552 ± 83
Astrocyte end-feet	OGB	30.9 ± 2.9	70.2 ± 10.6	27 ± 7	84 ± 8	682 ± 113
Neuropil	OGB	28.0 ± 2.7	92.9 ± 5.8	17 ± 4	65 ± 5	538 ± 75
Astrocyte processes	GCaMP6f	20.7 ± 2.7	41.7 ± 7.4	58 ± 14	99 ± 16	218 ± 37
Astrocyte = end-feet	GCaMP6f	18.9 ± 2.8	35.9 ± 8.0	67 ± 12	108 ± 15	249 ± 49
Fine astrocyte processes	GCaMP6f	5.0 ± 0.7	33.8 ± 6.8	79 ± 16	107 ± 18	202 ± 27

categories of pixels, astrocytic and nonastrocytic. Thus, four categories of POIs were initially included in the study: astrocyte processes, neuropil surrounding astrocyte processes, astrocyte end-feet, and neuropil surrounding the end-feet (Figure 2c). Using the POI method in combination with the analysis described previously (Lind et al., 2013), fast Ca^{2+} responses were observed in both astrocyte processes and end-feet and in the surrounding neuropil (Figure 2d). The level of significance was assessed relative to the s.d. within the baseline Ca^{2+} fluorescence activity ($F_{s.d.}$). A fast Ca^{2+} response was considered significant if its amplitude was >2 $F_{s.d.}$ and then evaluated for amplitude and timing (Figure 2e). The neuropil and astrocyte Ca^{2+} responses differed in several aspects. First, there were more responses in the neuropil than in the astrocytic areas (16.4 ± 7.9% more responses in neuropil than in astrocyte processes and 18 ± 9.6% more than in end-feet; Figure 2f and Table 1), whereas the magnitude of Ca^{2+} responses was slightly but significantly higher in astrocyte structures compared to neuropil (astrocyte processes 2.3 ± 1.6% and astrocyte end-feet 3.9 ± 1.2% higher than in neuropil; Figure 2g and Table 1). Finally, the neuropil Ca^{2+} responses preceded astrocyte responses with regard to onset time (astrocyte processes 13.7 ± 6.5 ms and astrocyte end-feet 10.8 ± 6.3 ms later than in neuropil), peak time (astrocyte processes 18.2 ± 6.5 ms and astrocyte end-feet 18.3 ± 5.0 ms later than in neuropil), and decay time (astrocyte processes 165.5 ± 90.8 ms and astrocyte end-feet 144.3 ± 83.5 ms later than in neuropil; Figure 2h and Table 1).

The triggering pathway for the rapid Ca^{2+} responses was verified in experiments using whisker stimulation with air puffs instead of electrical stimulation of the whisker pad. Ultra-short air puffs (0.2 ms) were applied in trains similar to the electrical stimulation and evoked Ca^{2+} increases in the same time scale in neuropil and astrocyte end-feet (Supporting Information Fig. S2a). Responses in astrocyte processes (Supporting Information Fig. S2b) were of the same size as in astrocyte end-feet and slightly larger than fast Ca^{2+} responses in the neuropil (Supporting Information Fig. S2c). To verify that the fast Ca^{2+} responses were indeed astrocytic, we used the genetically encoded Ca^{2+} indicator GCaMP6f driven by the short glial fibrillary acidic protein promoter (Movie M1, Supporting Information Fig. S3, and Figure 3). With this Ca^{2+} indicator, we observed fast Ca^{2+} responses in both astrocyte processes and end-feet. The fast Ca^{2+} increases in astrocyte end-feet preceded dilation of both penetrating arterioles (Supporting Information Movie M2, Figure 3a–c) and capillaries (Figure 3d–f). The Ca^{2+} responses were fewer (Figure 3g and Table 1) and smaller (Figure 3h and Table 1) than those measured with OGB. Most importantly, the timing of the responses was similar (Figure 3i and Table 1), and responses were clearly detectable in astrocyte structures. The difference can be explained by the difference in the concentration and K_d values of the two indicators (Chen et al., 2013). GCaMP6f was not expressed equally in all astrocyte end-feet; yet, fast Ca^{2+} increases occurred prior to dilation of 49% of penetrating arterioles and 56% of capillaries (Figure 3j). We did not observe any difference in the size, timing, or occurrence of Ca^{2+} responses in end-feet on arterioles versus on capillaries.

The use of a GECI allowed us to study the very fine astrocyte processes, gliapil, because these regions no longer contained a mixed signal from the astrocytes and neuronal dendrites. The Ca^{2+} responses measured in the gliapil were smaller (Figure 3h and Table 1) and slower (Figure 3i and Table 1) using GCaMP6F than OGB. This finding suggests that Ca^{2+} changes in neuronal dendrites, not gliapil, are the major contributors to the neuropil OGB signal. Another possible explanation is the low level of GCaMP6f expression in the gliapil compared to the larger structures (Supporting Information Fig. S4).

As the Ca^{2+} and blood flow responses to the whisker pad stimulation were physiological and, thus, frequency dependent, we studied pharmacological actions over a range of different stimulation frequencies. During the 15 s stimulation period, >2 Hz stimulation resulted in an attenuation of the fast Ca^{2+} responses (Lind et al., 2013). However, 3 Hz stimulation triggered the maximal blood flow response. The difference in dependence on stimulation frequency is reflected in the responses to 1 versus 3 Hz. This was apparent when we investigated whether the fast Ca^{2+} responses in astrocyte processes and end-feet are equally affected by pharmacological intervention of neuronal excitation and inhibition. The level of neuronal activation was studied via extracellular measurements of the fEPSP, which was measured as the negative amplitude of the LFP in the extracellular space (Jessen et al., 2014) and reflected in the neuropil Ca^{2+} activity. The nonastrocytic pixels surrounding the astrocyte processes were included as neuropil in this study (Figure 4a,e, upper row). The nonastrocytic pixels from the astrocyte end-feet sections were excluded because they encompassed both neuropil and vessel lumen pixels, although the results did not differ significantly from those obtained for the neuropil around astrocyte processes.

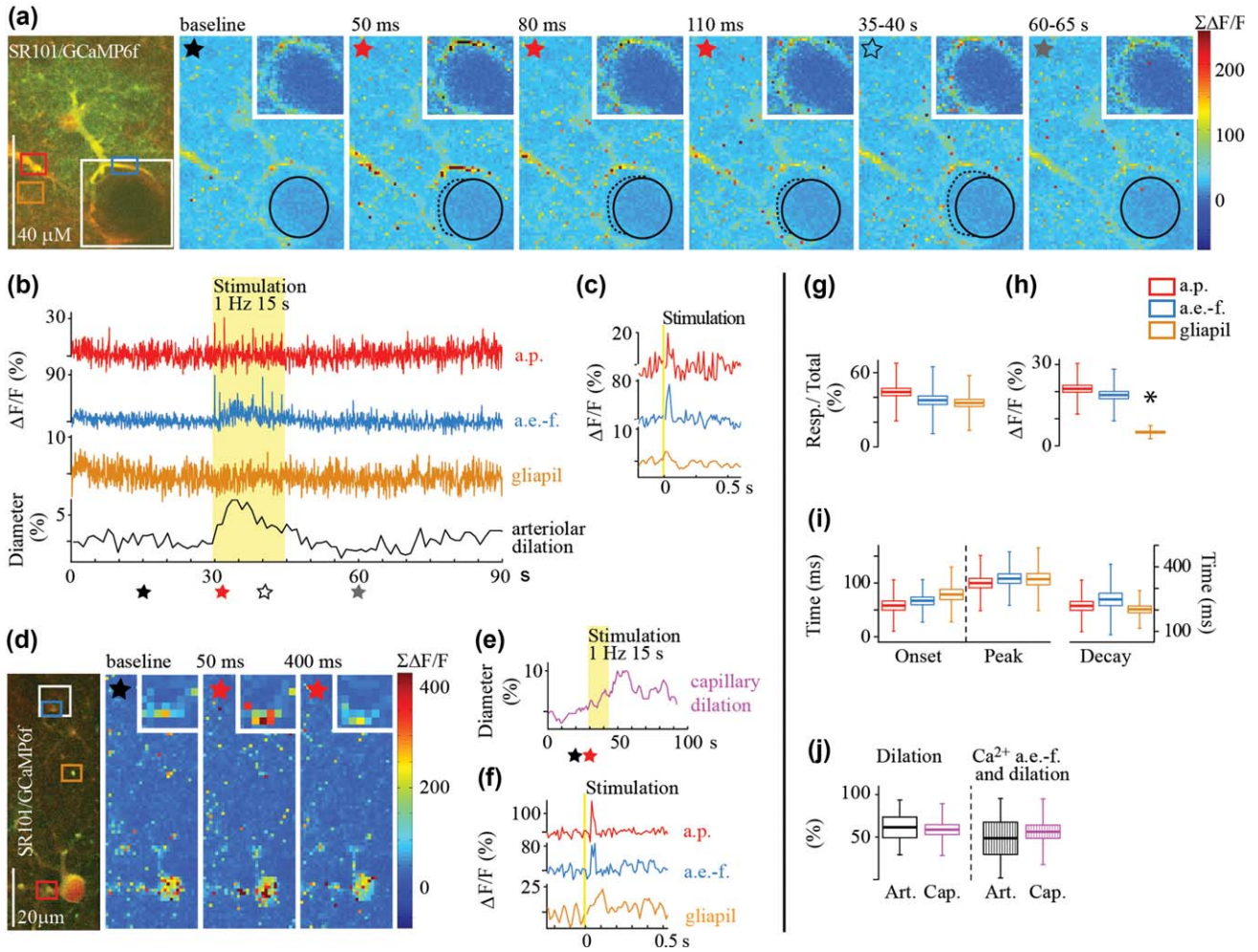

FIGURE 3 The fast Ca^{2+} signals in astrocyte processes and end-feet are cell type specific and precede dilation of penetrating arteriole and capillaries. (**a**) Fast Ca^{2+} signals in astrocytes were detected by the genetically encoded calcium indicator gfap-GCamP6f. Left, Combined GCaMP6f/SR101. Right, Ca^{2+} fluorescence summed over 30 ms at different time points before, during, and after stimulation. Stars in the upper corners of images refer to time points shown in the graph in (b). Penetrating arteriole is shown with dotted black line to mark the expansion and separately with no markings. (**b**) Ca^{2+} changes in the POIs selected in the squares marked in (a). The bottom graph depicts the change in diameter of the penetrating arteriole. (**c**) The fast Ca^{2+} signals calculated from each of the traces in (b). (**d**) GaMP6f/SR101 image with white box around capillary, shown enlarged in the upper right corner of images to the right. These show Ca^{2+} fluorescence summed over 30 ms before and during stimulation. (**e**) Dilation of the capillary in (d). (**f**) Fast Ca^{2+} responses in the POIs selected in the squares marked in (d) during the train of stimulations shown in (e). (**g–i**) The responsivity (g), maximal amplitude (h), and timing (i) of the fast Ca^{2+} responses measured in astrocyte processes, end-feet, and gliapil ($n = 40$ structures). (**j**) Dilating penetrating arterioles ($n = 7$) or capillaries ($n = 28$) during stimulation (open squares) and the percentage of vessels in which dilatation was preceded by a fast Ca^{2+} response in astrocyte end-feet (striped squares). Data are from 15 s, 0.5 Hz stimulations unless otherwise noted ($n = 10$ animals). Boxplots show mean (line), s.d. (box), and s.e.m. (whiskers). $^{*}p < 0.05$, $^{**}p < 0.01$, t-test

To target the excitatory system, two glutamate receptor antagonists blocking NMDAR or the AMPA receptor (AMPAR) were applied. MK801, which blocks NMDAR, did not reduce the fEPSP amplitudes (Figure 4c), but it did reduce the occurrence (Table 2) and the amplitude of the fast Ca^{2+} responses in the neuropil (Figure 4b, top). This effect was predictable due to the reduced influx of Ca^{2+} through NMDARs, but the effect on Ca^{2+} activity in astrocytes was unexpected. In the astrocyte processes, MK801 significantly reduced the amplitude (Figure 4b, middle) and responsiveness of POIs (Table 2). This influence of impaired NMDAR activation on Ca^{2+} responses in both neuropil and astrocyte processes associated the fast Ca^{2+} responses in astrocyte processes more closely with neuronal Ca^{2+} levels, which may be explained by the close association between astrocyte processes and the synapse.

In contrast, MK801 did not reduce the occurrence or magnitude of fast Ca^{2+} responses in the astrocyte end-feet (Figure 4b, bottom, and Table 2). Importantly, the stimulation-induced CBF responses were unaffected by MK801 (Figure 4d). This observation suggests that the stimulation-induced blood flow responses were independent of the fast Ca^{2+} responses in astrocyte processes and neuropil but covaried with the fast Ca^{2+} responses in astrocyte end-feet.

The AMPAR antagonist CNQX blocked synaptic transmission, as indicated by a marked reduction in the fEPSP amplitude for both 1 and

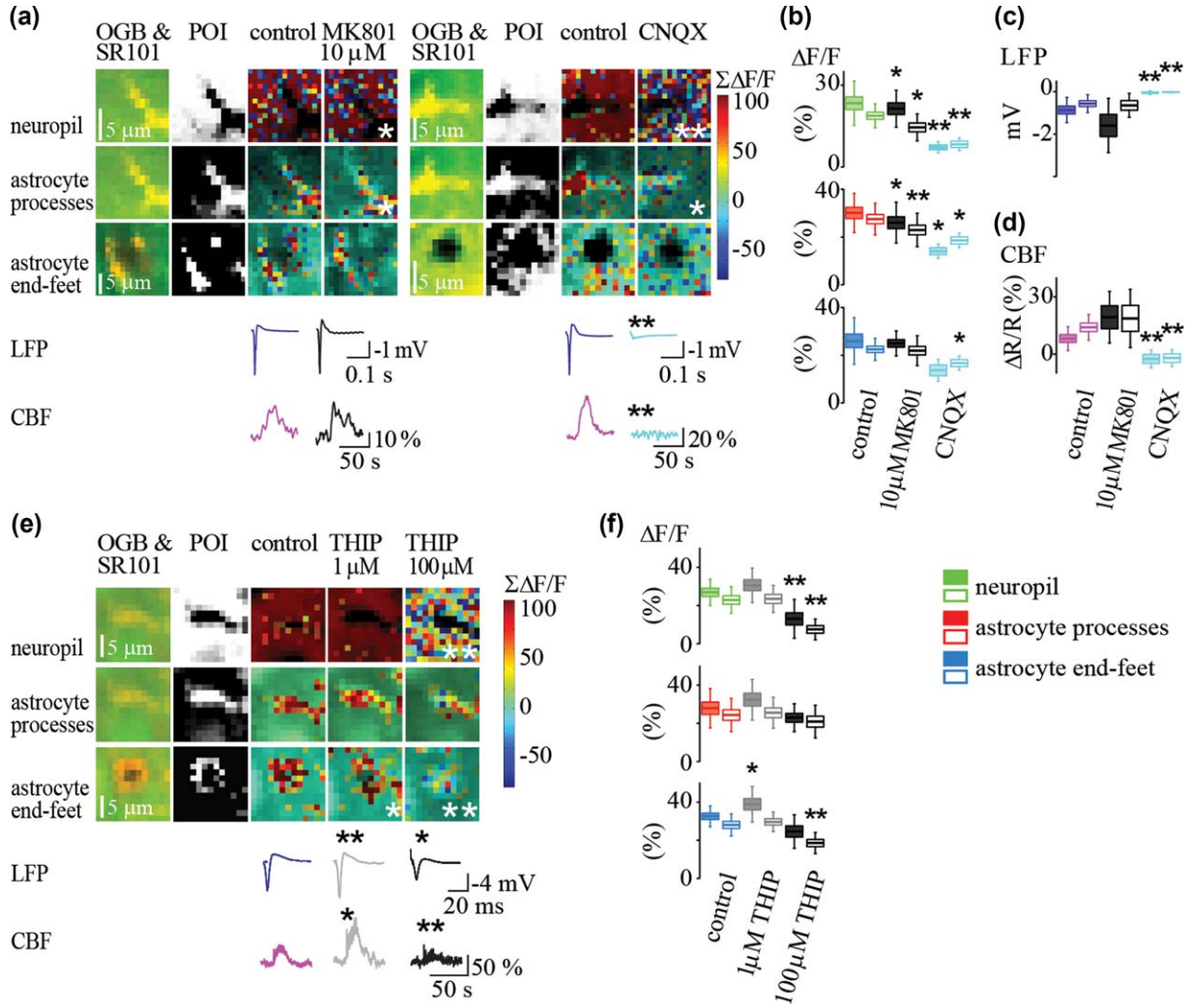

FIGURE 4 Modulation of synaptic activity, CBF, and fast-evoked Ca^{2+} signals via glutamate and $GABA_A$ receptors. The changes in blood flow closely follow the fast Ca^{2+} responses in astrocyte end-feet, whereas variations in the other two compartments are divergent. (**a**) Effect of the NMDAR antagonist MK801 and AMPAR antagonist CNQX on the fast Ca^{2+} changes in response to 1 Hz whisker pad stimulation in neuropil, astrocyte processes, and astrocyte end-feet. The Ca^{2+} responses were summed over 90 ms ($\Sigma\Delta F/F$). The traces show the effect on LFP and CBF responses. (**b**) Modulations of fast Ca^{2+} responses in neurons and astrocytes during 1 Hz stimulation frequency (filled squares, ■) or 3 Hz (open squares, □). The mean size of neuropil Ca^{2+} responses (top) was reduced by MK801 ($n = 12$) and CNQX ($n = 6$). MK801 ($n = 12$) and CNQX ($n = 6$) also reduced Ca^{2+} responses in astrocyte processes (middle row). In contrast, MK801 ($n = 12$) had no effect on fast Ca^{2+} responses in astrocyte end-feet (bottom), though CNQX did ($n = 6$). (**c**) CNQX reduced the size of fEPSPs ($n = 4$, $p < 1 \times 10^{-3}$, ANOVA; MK801: $n = 5$, $p = 0.562$, ANOVA), reflected in the depth of the amplitude of the LFPs. MK801 did not affect the fEPSPs (**d**) or reduce the size of the CBF response ($n = 5$, $p = 0.687$, ANOVA), which was significantly decreased by CNQX ($n = 4$, $p < 1 \times 10^{-3}$, ANOVA). (**e**) The effect of $GABA_AR$ agonist on fast Ca^{2+} signals in astrocyte end-feet was also reflected in the magnitude of the CBF responses. The images show the effect of two concentrations of THIP on the fast Ca^{2+} response in neuropil, astrocyte processes, and astrocyte end-feet during 15 s, 1 Hz stimulation. The LFP ($n = 13$) and CBF ($n = 8$) traces were averaged over 15 s, 1 Hz stimulations. At 1 μM, THIP reduced interneuron activity (Jessen et al., 2014), as reflected in larger fEPSPs ($n = 13$, 1 Hz: $p < 0.005$; 3 Hz: $p < 0.005$, t-test) and CBF responses ($n = 8$, 1 Hz: $p < 0.05$, *t*-test). At 100 μM, THIP reduced the activation of all neurons, leading to a reduction in the size of the fEPSPs ($n = 13$, 1 Hz: $p < 0.05$; 3 Hz: $p < 0.05$, *t*-test) and CBF responses ($n = 8$, 3 Hz: $p < 0.005$, *t*-test). (**f**) The maximum amplitude of the fast Ca^{2+} responses in neuropil (top) was significantly reduced by only 100 μM THIP ($n = 10$). THIP did not significantly reduce the amplitude of fast Ca^{2+} responses in astrocyte processes (middle panel), but in astrocyte end-feet (bottom) responses were significantly increased by 1 μM THIP ($n = 10$) and reduced by 100 μM THIP ($n = 10$). Boxplots show mean (line), s.d. (box), and s.e.m. (whiskers). $^*p < 0.05$, $^{**}p < 0.01$, *t*-test

3 Hz stimulation ($n = 4$, $p < 1 \times 10^{-3}$, both 1 and 3 Hz, *t*-test; Figure 4c). CNQX also removed most of the fast Ca^{2+} signals in the neuropil (Table 2) and reduced the amplitude (Figure 4b, top). Similar effects were observed on fast Ca^{2+} responses in astrocytes, with reduced amplitudes in astrocyte processes (Figure 4b, middle) and in end-feet (Figure 4b, bottom). Finally, the general reduction in activation introduced by AMPAR blockade was reflected in the absence of a CBF response to stimulation ($n = 4$, $p < 0.05$, both 1 and 3 Hz, *t*-test; Figure

TABLE 2 Difference in the percentage of responding POIs before and after drug application

		Astrocyte processes 1 Hz	Astrocyte processes 3 Hz	Astrocyte end-feet 1 Hz	Astrocyte end-feet 3 Hz	Neuropil 1 Hz	Neuropil 3 Hz
10 μM MK801	Max amplitude	13.6% ($p < 0.05$)	16.5% ($p < 0.01$)	3.8% ($p = 0.38$)	2.4% ($p = 0.80$)	8.6% ($p < 0.05$)	22.8% ($p < 0.05$)
10 μM MK801	Responsivity	18.8% ($p = 0.22$)	52% ($p < 0.05$)	29.8% ($p = 0.22$)	37.5% ($p = 0.24$)	1.4% ($p = 0.79$)	41.8% ($p < 0.01$)
CNQX	Max amplitude	53.2% ($p = 0.05$)	32.4% ($p < 0.05$)	47.3% ($p = 0.12$)	25.6% ($p < 0.05$)	73.9% ($p < 0.01$)	52.9% ($p < 0.01$)
CNQX	Responsivity	100% N.S. ANOVA	64% N.S. ANOVA	100% ($p = 0.12$)	62.5% ($p < 0.01$)	93.3% ($p < 0.01$)	73.33% ($p < 0.01$)
1 μM THIP	Max amplitude	−16.2% ($p = 0.17$)	−5% ($p = 0.55$)	−20% ($p < 0.05$)	−1.2% ($p = 0.35$)	−13.7% ($p = 0.39$)	−2.5% ($p = 0.80$)
1 μM THIP	Responsivity	0% ($p = 0.99$)	25% ($p = 0.16$)	−6.25% ($p = 0.43$)	15.4% ($p = 0.47$)	−8.0% ($p = 0.17$)	8.3% ($p = 0.20$)
100 μM THIP	Max amplitude	17.7% ($p = 0.13$)	14.1% ($p = 0.22$)	24% ($p = 0.06$)	36.7% ($p < 0.01$)	51.7% ($p < 0.01$)	67.3% ($p < 0.01$)
100 μM THIP	Responsivity	50%($p < 0.05$)	86.4% ($p < 0.01$)	43.8% ($p = 0.06$)	69.2% ($p < 0.05$)	58% ($p < 0.05$)	78.8% ($p < 0.01$)

Statistical analysis was carried out by three-way analysis of variance (ANOVA), followed by a paired *t*-test for significance at a specific stimulation frequency.
Abbreviation: (N.S. = not significant)

4d). Thus, both fast Ca^{2+} activity in astrocytes and CBF responses depended on intact synaptic input to the cortex.

Next, the inhibitory system of the whisker barrel cortex was targeted with THIP, which tonically activates extrasynaptic $GABA_AR$. The effect of THIP on CBF and EPSP was presented and discussed in our earlier work (Jessen et al., 2014). From that previous study, we knew that a 1 μM dose of THIP primarily affects inhibitory interneurons, leading to general disinhibition that is reflected in larger fEPSPs and CBF responses to 1 Hz whisker pad stimulation (raw data example in Figure 4e). In contrast, a higher dose of THIP (100 μM) suppresses excitatory neurons, resulting in diminution of fEPSP formation and CBF responses, especially at stimulation frequencies of 3 Hz. In this study, THIP at 1 μM increased the amplitude of the Ca^{2+} responses in astrocyte end-feet during 1 Hz stimulation (Figure 4f, bottom), but not significantly in the neuropil (Figure 4f, top) or astrocyte processes (Figure 4f, middle). The higher dose of 100 μM THIP significantly reduced the amplitude of the fast Ca^{2+} responses in the neuropil and astrocyte end-feet (Figure 4f), just as CBF and fEPSP responses were suppressed (Jessen et al., 2014). Thus, when the fast Ca^{2+} changes were studied in the presence of THIP, we observed a coupling between CBF responses and Ca^{2+} activity in the astrocyte end-feet.

4 | DISCUSSION

Here, we showed that fast Ca^{2+} responses can be detected in astrocyte processes using both chemical and genetically encoded Ca^{2+} indicators *in vivo* during somatosensory stimulation. We also found that different pharmacological interventions affect stimulation-induced fast Ca^{2+} responses in astrocyte end-feet and CBF responses to the same extent. Thus, we suggest that CBF responses may relate more to the fast Ca^{2+} activity in astrocyte end-feet than to Ca^{2+} responses in the neuropil and astrocyte processes. We described a novel method of investigating small astrocyte structures that is faster, less biased, and more optimal than when selecting ROIs based on visual evaluation.

This method involved the use of a pixel-based analysis to improve the evaluation of Ca^{2+} activity within small cellular structures. The quality of the method was assessed and compared to the ROI method commonly used for Ca^{2+} imaging. The POI method is relevant in studies using a fluorescent indicator that loads all types of cells equally, and cell specificity is achieved by counterstaining with a fluorescent marker for a specific cell or structure. In addition, the technique can be helpful in studying small structures. The method uses pixels that are selected from the average of several images, which improves the signal-to noise ratio and allows the study of Ca^{2+} changes in small structures at the limit of spatial resolution. The more precise definition of astrocytic areas gives assessment of Ca^{2+} responses in astrocyte processes and end-feet with higher sensitivity.

Astrocytes are known to compartmentalize; they have Ca^{2+} responses in microdomains (Asada et al., 2015; Bernardinelli et al., 2011), and isolated responses have been detected in both astrocyte processes (Di Castro et al., 2011; Panatier et al., 2011; Shigetomi et al., 2013) and end-feet (Girouard et al., 2010; Gordon et al., 2008; Petzold

et al., 2008). We observed that the fast Ca^{2+} responses in astrocyte processes and end-feet differed with regard to their dependence on NMDARs and $GABA_A$Rs. Moreover, Ca^{2+} activity in end-feet was more closely connected to changes in CBF than the activity in astrocyte processes. The difference in Ca^{2+} signaling in the two astrocyte compartments may be explained by the difference in associated structures. The structures defined as astrocyte end-feet were identified by their close connection to blood vessels, whereas astrocyte structures unrelated to blood vessels or close to the astrocyte soma were classified as processes. The astrocyte processes investigated here were among the largest branches, which successively split into numerous ultra-thin structures (Tong, Shigetomi, Looger, & Khakh, 2013). When OGB is used as the Ca^{2+} indicator, the very thin structures are inseparable from the neuropil, which consist of neuronal dendrites and processes. The Ca^{2+} signal from the neuropil is thought to primarily reflect the activity in neuronal dendrites (Dombeck, Khabbaz, Collman, Adelman, & Tank, 2007; Kerr & Denk, 2008; Lind et al., 2013). This notion is supported by our observation that the fast Ca^{2+} responses measured using the genetically encoded GCaMP6f in gliapil were small or nonexistent. The very small responses could also be due to a lower concentration of the genetically encoded Ca^{2+} indicator in these structures, as indicated by the low level of baseline fluorescence in the fine branches compared to larger branches of the astrocyte processes (Supporting Information Fig. S4). A sufficient level of Ca^{2+} indicator in a cell is essential for signal detection and responses may not be observed at low Ca^{2+} concentrations. Low levels of indicator due to suboptimal uptake and/or expression of the genetically encoded indicator in a proportion of astrocytes may also be the reason why fast Ca^{2+} responses were detected in only half of the astrocyte end-feet prior to vessel dilation. In contrast, a well-loaded chemical indicator enters all structures, giving more reliable expression levels and fluorescent responses. This can be an advantage when the effect of a drug is assessed as in Figure 4.

We observed that the Ca^{2+} responses from the neuropil and large astrocyte processes were similarly affected by the pharmacological interventions, reflecting a dependence of astrocytic Ca^{2+} levels on neuronal Ca^{2+} activity. A previous study of astrocytes described how neuronal activation triggers Ca^{2+} responses in gliapil, which then propagate to the larger cell structures (Kanemaru et al., 2014). NMDAR activation is a major source of neuronal Ca^{2+} elevation (Chalifoux & Carter, 2011; Sabatini, Oertner, & Svoboda, 2002), which explains the attenuating effect of MK801 on the fast Ca^{2+} responses in the neuropil. Similar attenuation was observed in astrocyte processes, possibly indicating that Ca^{2+} activity in astrocyte processes reflects activity in the synapses that they surround, and potentially post-synaptic Ca^{2+} (Di Castro et al., 2011; Panatier et al., 2011). The effects of the glutamate receptor antagonist and $GABA_A$R agonist on the fast astrocytic Ca^{2+} response are likely to be explained by an indirect effect via the suppression of neuronal activity. The effect of CNQX reflects postsynaptic blockade in layer II/III neurons, in addition to silencing of the synaptic input from layer IV. Thus, the effect of the AMPAR antagonist on fEPSP, Ca^{2+}, and CBF responses was predictable, as CNQX blocks all activities upstream from a synaptic input.

Though the cellular mechanism leading to fast Ca^{2+} responses in astrocytes is not completely understood, some studies have reported a loss of the slow evoked Ca^{2+} signals in astrocyte IP_3R knockout (KO) animals (Di Castro et al., 2011; Kanemaru et al., 2014; Nizar et al., 2013). These mice had intact neurovascular coupling despite the astrocytes lacking IP_3R (Bonder & McCarthy, 2014; Nizar et al., 2013) and dilation of blood vessels without obvious changes in Ca^{2+} levels (Institoris, Rosenegger, & Gordon, 2015). Interestingly, a more recent study showed intact Ca^{2+} responses in astrocyte processes in IP_3R KO animals (Rungta et al., 2016; Srinivasan et al., 2015). In addition, other studies maintain that Ca^{2+} in astrocyte processes and end-feet plays a role in CBF regulation (Biesecker & Srienc, 2015; Dunn et al., 2013; Otsu et al., 2015), which our results tend to support. These conflicting results may have been conciliated by two recent studies showing how astrocytic Ca^{2+} changes are essential for the dilation of capillaries, but not arterioles (Biesecker et al., 2016; Mishra et al., 2016). Thus, when a fast Ca^{2+} change was observed in the current study in end-feet surrounding both capillaries and arterioles, only those in the capillaries can be expected to have an effect on vessel diameter. The effects of the different pharmacological modifications on astrocytic Ca^{2+} support a regulatory role on CBF. Although MK801 reduced the fast Ca^{2+} responses in the neuropil and astrocyte processes in the current study, fast Ca^{2+} responses were preserved in the astrocyte end-feet. Similarly, the sizes of the fEPSP and CBF responses were unchanged. The same dose of MK801 was previously shown to reduce CBF responses to stimulation of the whisker barrel cortex in rats (Nielsen & Lauritzen, 2001), but much higher doses are required to reduce the CBF in mice (Toussay, Basu, Lacoste, & Hamel, 2013). Low dose of the extrasynaptic $GABA_A$R agonist increased fEPSPs and augmented CBF responses during low-frequency stimulation because of an inhibition of inhibitory interneurons (Jessen et al., 2014). The result is disinhibition, which was also observed in this study with the significantly increased fast Ca^{2+} responses in astrocyte end-feet during low stimulation frequencies. This effect suggests the participation of interneurons in the regulation of end-feet activity, as inhibitory interneurons terminate on astrocytes close to the vessels (Hamel, 2006) and contribute to astrocytic Ca^{2+} responses (Doengi, Deitmer, & Lohr, 2008; Simard, Arcuino, Takano, Liu, & Nedergaard, 2003). A complete blood flow response has been found to depend on the activity of both inhibitory interneurons and astrocytes (Lecrux et al., 2011). In slices, vasointestinal peptide and somatostatin released from interneurons stimulate Ca^{2+} responses in astrocyte end-feet prior to vasodilation (Straub, Bonev, Wilkerson, & Nelson, 2006). These results support the hypothesis that astrocyte end-feet function as a separate entity (Nuriya & Yasui, 2013) and could explain why the fast Ca^{2+} responses in the current study were less sensitive to MK801 but more susceptible to activation of the extrasynaptic $GABA_A$Rs. High dose THIP (100 μM) reduced CBF and fEPSP responses (Jessen et al., 2014) in accordance with a reduced fast Ca^{2+} response in astrocyte end-feet. A similar dose of THIP depolarizes astrocytes in hippocampal slices, blocking the two-pore domain K^+ channels (Ma, Xie, & Zhou, 2012) and the release of vasodilator K^+.

In summary, fast Ca^{2+} responses in astrocyte end-feet correlated with CBF responses to the stimulation of the whisker barrel cortex.

These results do not clarify the mechanism, but our modifications of the system led us to establish that the fast Ca^{2+} responses occur in astrocyte end-feet and contribute to neurovascular coupling.

ACKNOWLEDGMENT

This study was supported by the Lundbeck Foundation, the NOVO-Nordisk Foundation, the Danish Medical Research Council, the NORDEA Foundation for the Center for Healthy Aging, and Fondation Leducq. None of the authors have any conflicts of interest to declare.

ORCID

Barbara Lykke Lind http://orcid.org/0000-0003-0027-5226

REFERENCES

Asada, A., Ujita, S., Nakayama, R., Oba, S., Ishii, S., Matsuki, N., & Ikegaya, Y. (2015). Subtle modulation of ongoing calcium dynamics in astrocytic microdomains by sensory inputs. *Physiological Reports*, *3*, pii: e12454. doi: 10.14814/phy2.12454.

Attwell, D., Buchan, A. M., Charpak, S., Lauritzen, M., MacVicar, B. A., & Newman, E. A. (2010). Glial and neuronal control of brain blood flow. *Nature*, *468*, 232–243.

Bernardinelli, Y., Salmon, C., Jones, E. V., Farmer, W. T., Stellwagen, D., & Murai, K. K. (2011). Astrocytes display complex and localized calcium responses to single-neuron stimulation in the hippocampus. *Journal of Neuroscience*, *31*, 8905–8919.

Biesecker, K. R., & Srienc, A. I. (2015). The functional role of astrocyte calcium signaling in cortical blood flow regulation. *Journal of Neuroscience*, *35*:868–870.

Biesecker, K. R., Srienc, A. I., Shimoda, A. M., Agarwal, A., Bergles, D. E., Kofuji, P., & Newman, E. A. (2016). Glial cell calcium signaling mediates capillary regulation of blood flow in the retina. *Journal of Neuroscience*, *36*, 9435–9445.

Bindocci, E., Savtchouk, I., Liaudet, N., Becker, D., Carriero, G., & Volterra, A. (2017). Three-dimensional Ca2+ imaging advances understanding of astrocyte biology. *Science 356*, pii: eaai8185.

Bonder, D. E., & McCarthy, K. D. (2014). Astrocytic Gq-GPCR-linked IP3R-dependent Ca2+ signaling does not mediate neurovascular coupling in mouse visual cortex in vivo. *Journal of Neuroscience*, *34*, 13139–13150.

Chalifoux, J. R., & Carter, A. G. (2011). Glutamate spillover promotes the generation of NMDA spikes. *Journal of Neuroscience*, *31*, 16435–16446.

Chen, T. W., Wardill, T. J., Sun, Y., Pulver, S. R., Renninger, S. L., Baohan, A., … Kim, D. S. (2013). Ultrasensitive fluorescent proteins for imaging neuronal activity. *Nature*, *499*, 295–300.

Devor, A., Dunn, A. K., Andermann, M. L., Ulbert, I., Boas, D. A., & Dale, A. M. (2003). Coupling of total hemoglobin concentration, oxygenation, and neural activity in rat somatosensory cortex. *Neuron*, *39*, 353–359.

Di Castro, M. A., Chuquet, J., Liaudet, N., Bhaukaurally, K., Santello, M., Bouvier, D., … Volterra, A. (2011). Local Ca2+ detection and modulation of synaptic release by astrocytes. *Nature Neuroscience*, *14*, 1276–1284.

Doengi, M., Deitmer, J. W., & Lohr, C. (2008). New evidence for purinergic signaling in the olfactory bulb: A2A and P2Y1 receptors mediate intracellular calcium release in astrocytes. *FASEB Journal*, *22*, 2368–2378.

Dombeck, D. A., Khabbaz, A. N., Collman, F., Adelman, T. L., & Tank, D. W. (2007). Imaging large-scale neural activity with cellular resolution in awake, mobile mice. *Neuron*, *56*, 43–57.

Dunn, K. M., Hill-Eubanks, D. C., Liedtke, W. B., & Nelson, M. T. (2013). TRPV4 channels stimulate Ca2+-induced Ca2+ release in astrocytic endfeet and amplify neurovascular coupling responses. *Proceedings of the National Academy of Sciences U S A 110*, 6157–6162.

Girouard, H., Bonev, A. D., Hannah, R. M., Meredith, A., Aldrich, R. W., & Nelson, M. T. (2010). Astrocytic endfoot Ca2+ and BK channels determine both arteriolar dilation and constriction. *Proceedings of the National Academy of Sciences U S A 107*:3811–3816.

Gordon, G. R., Choi, H. B., Rungta, R. L., Ellis-Davies, G. C., & MacVicar, B. A. (2008). Brain metabolism dictates the polarity of astrocyte control over arterioles. *Nature*, *456*, 745–749.

Hamel, E. (2006). Perivascular nerves and the regulation of cerebrovascular tone. *Journal of Applied Physiology*, *100*, 1059–1064.

Howarth, C. (2014). The contribution of astrocytes to the regulation of cerebral blood flow. *Frontiers in Neuroscience*, *8*, 103.

Iadecola, C., & Nedergaard, M. (2007). Glial regulation of the cerebral microvasculature. *Nature Neuroscience*, *10*, 1369–1376.

Institoris, A., Rosenegger, D. G., & Gordon, G. R. (2015). Arteriole dilation to synaptic activation that is sub-threshold to astrocyte endfoot Ca transients. *Journal of Cerebral Blood Flow and Metabolism*, *35*(9), 1411–1415.

Jessen, S. B., Brazhe, A., Lind, B. L., Mathiesen, C., Thomsen, K., Jensen, K., & Lauritzen, M. (2014). GABAA Receptor-Mediated Bidirectional Control of Synaptic Activity, Intracellular Ca2+, Cerebral Blood Flow, and Oxygen Consumption in Mouse Somatosensory Cortex In Vivo. *Cerebral Cortex*, *25*(9), 2594–2609.

Kacem, K., Lacombe, P., Seylaz, J., & Bonvento, G. (1998). Structural organization of the perivascular astrocyte endfeet and their relationship with the endothelial glucose transporter: A confocal microscopy study. *Glia*, *23*, 1–10.

Kanemaru, K., Sekiya, H., Xu, M., Satoh, K., Kitajima, N., Yoshida, K., … Tanaka, K. F. (2014). In vivo visualization of subtle, transient, and local activity of astrocytes using an ultrasensitive Ca(2+) indicator. *Cell Reports*, *8*, 311–318.

Kerr, J. N., & Denk, W. (2008). Imaging in vivo: Watching the brain in action. *Nature Reviews. Neuroscience*, *9*, 195–205.

Lauritzen, M., Mathiesen, C., Schaefer, K., & Thomsen, K. J. (2012). Neuronal inhibition and excitation, and the dichotomic control of brain hemodynamic and oxygen responses. *Neuroimage*, *62*, 1040–1050.

Lecrux, C., Toussay, X., Kocharyan, A., Fernandes, P., Neupane, S., Levesque, M., … Hamel, E. (2011). Pyramidal neurons are "neurogenic hubs" in the neurovascular coupling response to whisker stimulation. *Journal of Neuroscience*, *31*, 9836–9847.

Lind, B. L., Brazhe, A. R., Jessen, S. B., Tan, F. C., & Lauritzen, M. J. (2013). Rapid stimulus-evoked astrocyte Ca2+ elevations and hemodynamic responses in mouse somatosensory cortex in vivo. *Proceedings of the National Academy of Sciences of the United States of America*, *110*, E4678–4687.

Logothetis, N. K., Pauls, J., Augath, M., Trinath, T., & Oeltermann, A. (2001). Neurophysiological investigation of the basis of the fMRI signal. *Nature*, *412*, 150–157.

Ma, B. F., Xie, M. J, & Zhou, M. (2012). Bicarbonate efflux via GABA(A) receptors depolarizes membrane potential and inhibits two-pore domain potassium channels of astrocytes in rat hippocampal slices. *Glia*, *60*, 1761–1772.

McCaslin, A. F., Chen, B. R., Radosevich, A. J., Cauli, B., & Hillman, E. M. (2011). In vivo 3D morphology of astrocyte-vasculature interactions in the somatosensory cortex: Implications for neurovascular coupling. *Journal of Cerebral Blood Flow and Metabolism*, *31*, 795–806.

Mishra, A., Reynolds, J. P., Chen, Y., Gourine, A. V., Rusakov, D. A., & Attwell, D. (2016). Astrocytes mediate neurovascular signaling to capillary pericytes but not to arterioles. *Nature Neuroscience*, *19*, 1619–1627.

Nielsen, A., & Lauritzen, M. (2001). Coupling and uncoupling of activity-dependent increases of neuronal activity and blood flow in rat somatosensory cortex. *The Journal of Physiology*, *533*, 773–785.

Nimmerjahn, A. (2009). Astrocytes going live: advances and challenges. *The Journal of Physiology*, *587*, 1639–1647.

Nizar, K., Uhlirova, H., Tian, P., Saisan, P. A., Cheng, Q., Reznichenko, L., … Devor, A. (2013). In vivo Stimulus-Induced Vasodilation Occurs without IP3 Receptor Activation and May Precede Astrocytic Calcium Increase. *The Journal of Neuroscience*, *33*, 8411–8422.

Nuriya, M., & Yasui, M. (2013). Endfeet serve as diffusion-limited subcellular compartments in astrocytes. *Journal of Neuroscience*, *33*, 3692–3698.

Otsu, Y., Couchman, K., Lyons, D. G., Collot, M., Agarwal, A., Mallet, J. M., … Charpak, S. (2015). Calcium dynamics in astrocyte processes during neurovascular coupling. *Nature Neuroscience*, *18*, 210–218.

Panatier, A., Vallee, J., Haber, M., Murai, K. K., Lacaille, J. C., & Robitaille, R. (2011). Astrocytes are endogenous regulators of basal transmission at central synapses. *Cell*, *146*, 785–798.

Petzold, G. C., Albeanu, D. F., Sato, T. F., & Murthy, V. N. (2008). Coupling of neural activity to blood flow in olfactory glomeruli is mediated by astrocytic pathways. *Neuron*, *58*, 897–910.

Raichle, M. E., & Mintun, M. A. (2006). Brain work and brain imaging. *Annual Review of Neuroscience*, *29*, 449–476.

Reeves, A. M. B., Shigetomi, E., & Khakh, B. S. (2011). Bulk loading of calcium indicator dyes to study astrocyte physiology: Key limitations and improvements using morphological maps. *The Journal of Neuroscience*, *31*, 9353–9358.

Rungta, R. L., Bernier, L. P., Dissing-Olesen, L., Groten, C. J., LeDue, J. M., Ko, R., … MacVicar, B. A. (2016). Ca2+ transients in astrocyte fine processes occur via Ca2+ influx in the adult mouse hippocampus. *Glia*, *64*, 2093–2103.

Sabatini, B. L., Oertner, T. G., & Svoboda, K. (2002). The life cycle of Ca (2+) ions in dendritic spines. *Neuron*, *33*, 439–452.

Shigetomi, E., Bushong, E. A., Haustein, M. D., Tong, X., Jackson-Weaver, O., Kracun, S., … Khakh, B. S. (2013). Imaging calcium microdomains within entire astrocyte territories and endfeet with GCaMPs expressed using adeno-associated viruses. *Journal of General Physiology*, *141*, 633–647.

Simard, M., Arcuino, G., Takano, T., Liu, Q. S., & Nedergaard, M. (2003). Signaling at the gliovascular interface. *Journal of Neuroscience*, *23*, 9254–9262.

Srinivasan, R., Huang, B. S., Venugopal, S., Johnston, A. D., Chai, H., Zeng, H., … Khakh, B. S. (2015). Ca(2+) signaling in astrocytes from Ip3r2(-/-) mice in brain slices and during startle responses in vivo. *Nature Neuroscience*, *18*, 708–717.

Stobart, J., Ferrari, K. D., Barrett, M. J. P., Stobart, M. J., Looser, Z. J., Saab, A. S., & Weber, B. (2016). Long-term in vivo calcium imaging of astrocytes reveals distinct cellular compartment responses to sensory stimulation. *Cerebral Cortex*, 1–15.

Straub, S. V., Bonev, A. D., Wilkerson, M. K., & Nelson, M. T. (2006). Dynamic inositol trisphosphate-mediated calcium signals within astrocytic endfeet underlie vasodilation of cerebral arterioles. *Journal of General Physiology*, *128*, 659–669.

Tong, X., Shigetomi, E., Looger, L. L., & Khakh, B. S. (2013). Genetically encoded calcium indicators and astrocyte calcium microdomains. *Neuroscientist*, *19*, 274–291.

Toussay, X., Basu, K., Lacoste, B., & Hamel, E. (2013). Locus coeruleus stimulation recruits a broad cortical neuronal network and increases cortical perfusion. *Journal of Neuroscience*, *33*, 3390–3401.

Verkhratsky, A., Rodriguez, J. J., & Parpura, V. (2012). Calcium signalling in astroglia. *Molecular and Cellular Endocrinology*, *353*, 45–56.

Volterra, A., Liaudet, N., & Savtchouk, I. (2014). Astrocyte Ca(2)(+) signalling: An unexpected complexity. *Nature Reviews. Neuroscience*, *15*, 327–335.

Winship, I. R., Plaa, N., & Murphy, T. H. (2007). Rapid astrocyte calcium signals correlate with neuronal activity and onset of the hemodynamic response in vivo. *Journal of Neuroscience*, *27*, 6268–6272.

SUPPORTING INFORMATION

Additional Supporting Information may be found online in the supporting information tab for this article.

How to cite this article: Lind BL, Jessen SB, Lønstrup M, Joséphine C, Bonvento G, Lauritzen M. Fast Ca^{2+} responses in astrocyte end-feet and neurovascular coupling in mice. *Glia*. 2017;00:1–11. https://doi.org/10.1002/glia.23246